RESEARCH ARTICLE

Elucidating the Role of Mass Transfer in Electrochemical Redox Reactions on Electrospun Fibers

Yan Li[1] · Ziwang Kan[1] · Lina Jia[1] · Dan Zhang[1] · Yan Hong[1] · Jingjing Liu[1] · Haibo Huang[2] · Siqi Li[1] · Song Liu[1]

Abstract

Mass transfer can tune the surface concentration of reactants and products and subsequently influence the catalytic performance. The morphology of nanomaterials plays an important role in the mass transfer of reaction microdomains, but related studies are lacking. Herein, a facile electrospinning technique utilizing cellulose was employed to fabricate a series of carbon nanofibers with different diameters, which exhibited excellent electrochemical nitrate reduction reaction and oxygen evolution reaction activities. Furthermore, the microstructure of electrocatalysts could influence the gas–liquid–solid interfacial mass transfer, resulting in different electrochemical performances.

Graphical abstract
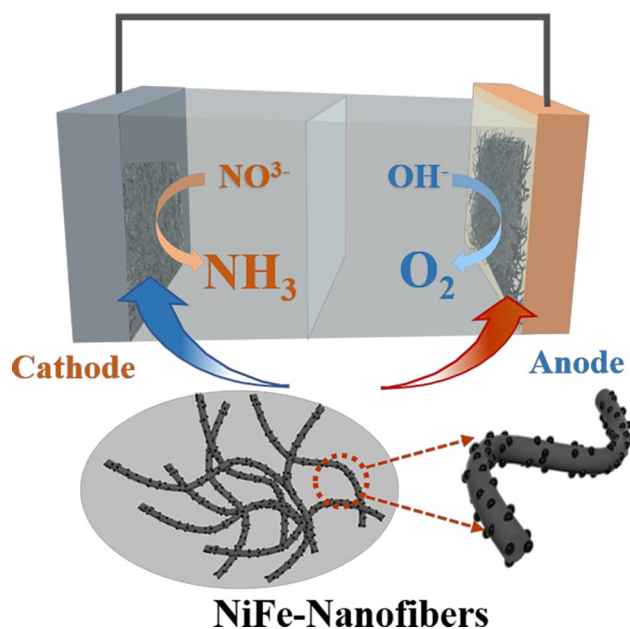
Yan Li, Ziwang Kan and Lina Jia contribute equally to this work.

Extended author information available on the last page of the article

Introduction

Electrochemical nitrate reduction reaction (NO_3RR) offers a promising solution to reduce nitrate pollution and produce high-value-added ammonia (NH_3) [1–3]. However, the NO_3RR is kinetically sluggish, with the overpotential being usually exceeding 1 V [4–6]. Furthermore, the large driving force of the anodic oxygen evolution reaction (OER) prevents the NO_3RR from being applied on a large scale [7–9]. Therefore, tremendous efforts have been made to develop highly efficient NO_3RR and OER electrocatalysts [10, 11]. Non-noble transition metal catalysts are the ideal choice owing to their low cost, high efficiency, and easy modification [12–16].

The charge transfer steps are usually the rate determining step in the NO_3RR and OER [17–20]. However, the mass transfer steps are more likely to control the reaction rate at the high overpotential [21, 22]. Therefore, understanding the influence of the mass transfer in the NO_3RR and OER is important for further large-scale industrial applications. The nitrate and ammonium ion transfer primarily involves the liquid and solid phases in the NO_3RR. Furthermore, the oxygen transfer requires gas, liquid, and solid phases. One-dimensional (1D) nanomaterials exhibit outstanding mass transfer properties owing to the plenty of open spaces among the adjacent 1D nanostructure. He et al. [23] found that the copper/cobalt array could efficiently convert NO_3^- to NH_3. Furthermore, the current density was large because the mass transfer was excellent. Liu et al. [24] demonstrated that the 1D carbon nanotube can enhance the OER performance of the CoMn-layered double hydroxides. This may be because of the easier diffusion of oxygen from the surface of the as-prepared nanomaterials. Thus, achieving the high NO_3RR and OER activity by designing 1D nanomaterials with different microstructures is promising. Furthermore, it is essential to determine how the 1D microstructure influences interfacial mass transfer. The electrospinning could easily change the 1D structure by adjusting the related parameters, such as voltage, distance, and viscosity [25–27].

In this research, we systematically investigated the influence of the gas–liquid–solid triphase interfacial mass transfer on the NO_3RR and the OER using a series of nickel and iron-loaded nanofibers (NiFe-NFs) materials, which were synthesized via electrospinning and pyrolysis methods. The diameter of the as-prepared 1D NFs could be controllably adjusted by varying the preoxidative heating rate. Among these nanomaterials, the NiFe-NFs-2 (under pre-oxidative heating rate of 2 °C/min) displayed a surprising NO_3RR activity, a Faradaic efficiency of 94.3%, and a large NH_3 yield of 10,489 µg/(h·mg), showing an excellent OER performance with an overpotential of 307 mV at the current density of 10 mA/cm² and a small Tafel slope of 44.3 mV/

dec. Experiments and theoretical calculations indicated that the diameter of the 1D NFs could change the reactant transfer, thereby improving the electrochemical performance.

Results and Discussion

The NiFe-NFs were synthesized via electrospinning and two-step heat treatment (Fig. 1a). First, the precursor NFs were prepared via electrospinning and were then preoxidized at 250 °C in air atmosphere and carbonized at 800 °C in an Ar/H_2 atmosphere to obtain NiFe-NFs. The heating rate during the preoxidation could control the diameter of the NiFe-NFs. Thus, the different heating rates of 1 °C/min, 2 °C/min, 3 °C/min, 4 °C/min and 5 °C/min were applied during the synthesis process, and the as-prepared NiFe-NFs were named NiFe-NFs-X ($X = 1, 2, 3, 4, 5$; X represents the heating rate of preoxidation).

Scanning electron microscopy (SEM) was used to analyze NiFe-NFs-X (Figs. S1, S2) to confirm the effect of the preoxidation rate on the catalyst morphology. The precursor NFs displayed a smooth surface with a uniform diameter of ~ 300 nm (Figs. S1, S2). After the preoxidation, the gas released during the precursor nanofibers crystallizes and decomposes, and the diameter of the NFs was considerably reduced with the different preoxidation heating rates (Fig. S2). With the decrease in the preoxidation rate, the diameter of NFs gradually decreases. The preoxidation heating rate of 2 °C/min makes the diameter of the NFs smaller. The carbonization further reduced the diameter of the NFs and exposed the NiFe nanoparticles to varying degrees. The SEM images revealed that the NiFe-NFs-2 has the smallest diameter of NFs with an average diameter of 45.3 nm (Figs. 1b, S3). Transmission electron microscopy (TEM) images (Figs. S4, 1c) revealed that the average nanoparticle size of NiFe-NFs-2 is ~ 24.65 nm, which is considerably smaller than those of other catalysts. Notably, the combination of NFs and nanoparticles in NiFe-NFs-X creates a rough surface structure that considerably increases the specific surface area of the catalyst and facilitates the mass transfer process of the reaction. Among them, NiFe-NFs-2 has the roughest surface structure, and it is speculated that it possesses better catalytic activity.

Furthermore, the high-resolution transmission electron microscopy (HRTEM) image revealed the lattice fringes at 0.213 nm and 0.185 nm assigned to the facets (111) and (002) of NiFe alloy, respectively. The X-ray diffraction (XRD) pattern of NiFe-NFs further confirmed the presence of NiFe nanoparticles on the nanomaterials. Prominent diffraction peaks $2\theta = 43.76°$ and 50.92° matched the standard NiFe peaks (PDF No.98-063-2933) (Fig. 1e). Moreover, the C peak at 25° gradually decreased with decreasing rate of NiFe-NFs-X preoxidation. This is primarily due to the

Fig. 1 **a** Schematic of the NiFe-NFs-*X* synthesis process. **b** SEM image of NiFe-NFs-2, the inset shows the diameter distribution of nanofibers. **c** TEM image of NiFe-NFs-2 in the inset shows the diameter distribution of nanoparticles. **d** HRTEM image of NiFe-NFs-2. **e** XRD patterns, **f** Raman spectrum, and **g** TG curves of as-prepared samples
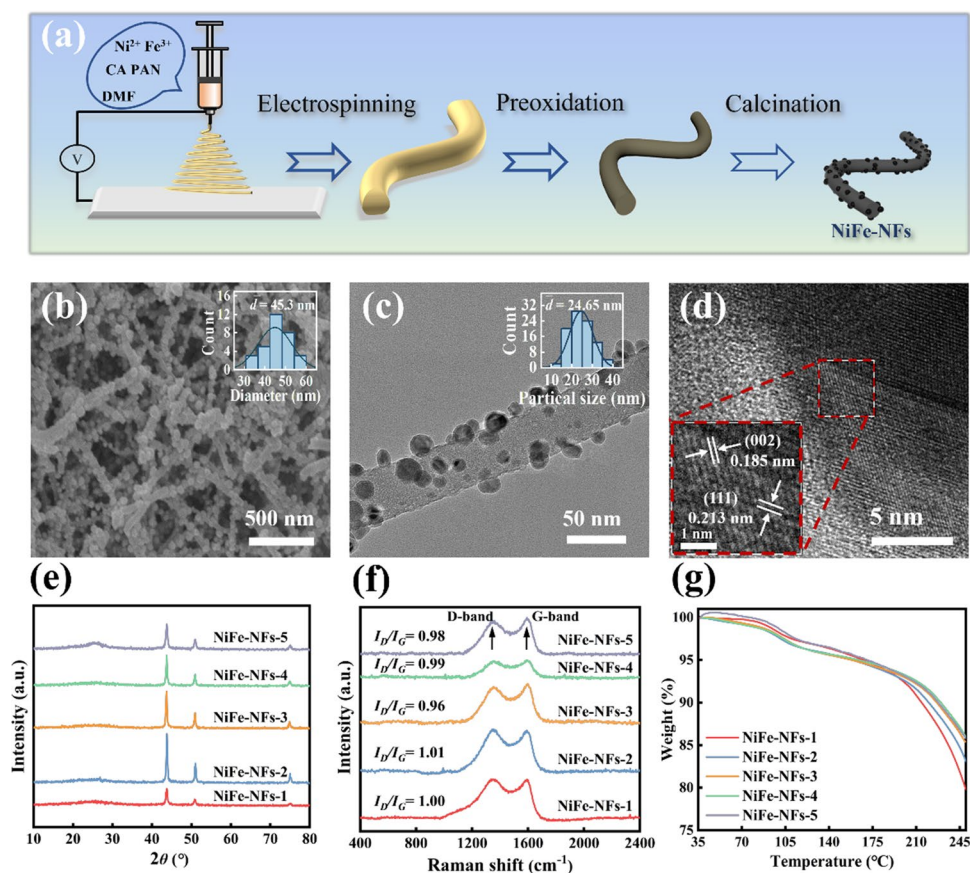

large number of NiFe nanoparticles covering the catalyst surface, which weakened the intensity of the C peak signal. The Raman spectrum of NiFe-NFs-*X* revealed two peaks at 1300 and 1580 cm^{-1} corresponding to the D and G bands of the carbon materials. The intensity ratios I_D/I_G of NiFe-NFs-*X* were similar (Fig. 1f), implying that the graphitization degrees of the samples were similar. The preoxidation heating of precursor NFs was studied using the thermogravimetric (TG) method. The calcined TG curves depicted the fiber heating to 250 °C in air atmosphere at varying heating rates ranging from 1 to 5 °C/min (Fig. 1g). TG curves revealed that the weight loss rate was inversely proportional to the preoxidation heating rate, implying that the fiber weight loss rate was smaller at a larger heating rate. This is primarily because the preoxidation process increases the amount of C–O and C=O on the catalyst surface, and the slower the heating rate, the higher the preoxidation degree and, thus, the greater the weight loss rate. Therefore, the surface roughness increases with decreasing heating rate from 2 to 5 °C. However, with a further decrease in heating rate, the particles will be considerably exposed, and the roughness will decrease due to agglomeration at high temperatures.

To further determine the chemical composition and elemental states of NiFe-NFs, X-ray photoelectron spectroscopy (XPS) was performed. The characteristic signatures for C, O, N, Ni, and Fe element were visible in the survey scan spectrum of NiFe-NFs-*X* (Fig. S5). Table S1 presents the atomic ratio of NiFe-NFs-*X*. Compared to other catalysts, NiFe-NFs-2 has the highest Ni and Fe content (Ni: 16.64% and Fe: 11.85%) and the lowest C content (C: 42.92%), indicating that the NiFe nanoparticles are fully exposed to the C surface. The C 1s spectrum of NiFe-NFs-*X* reveals four fitted peaks located at 284.8, 285.6, 286.9, and 289.2 eV corresponding to C=C, C–N, C=O, and C–O, respectively (Figs. 2a, S6a–d) [28–30]. The decomposition of the N 1 s spectrum of NiFe-NFs-*X* is fitted with three peaks at 398.3, 399.3, and 400.8 eV corresponding to pyridinic N, pyrrolic N, and graphitic N, respectively (Figs. 2b, S7a–d) [31, 32]. The Ni 2p spectrum of NiFe-NFs-*X* deconvoluted into Ni^0 (852.9 and 870.1 eV) and Ni^{2+} (855.6 and 873.6 eV) (Figs. 2c, S8a–d) [33–35]. The Fe 2p spectrum of NiFe-NFs-*X* deconvoluted into Fe^0 (707.4 and 720.5 eV), Fe^{2+} (710.3 and 723.8 eV), and Fe^{3+} (712.5 and 725.1 eV) (Figs. 2d, S9a–d) [36–38]. The XPS results revealed that the C 1s and N 1s regions of NiFe-NFs-*X* are similar, indicating the consistent in properties of carbon NFs [28]. When comparing NiFe-NFs-2 with NiFe-NFs-*X*, the peaks of Ni^0 and Fe^0 were more prominent. This is primarily due to the NFs of NiFe-NFs-2 and the exposed NiFe nanoparticles are more easily reduced by Ar/H$_2$ gas.
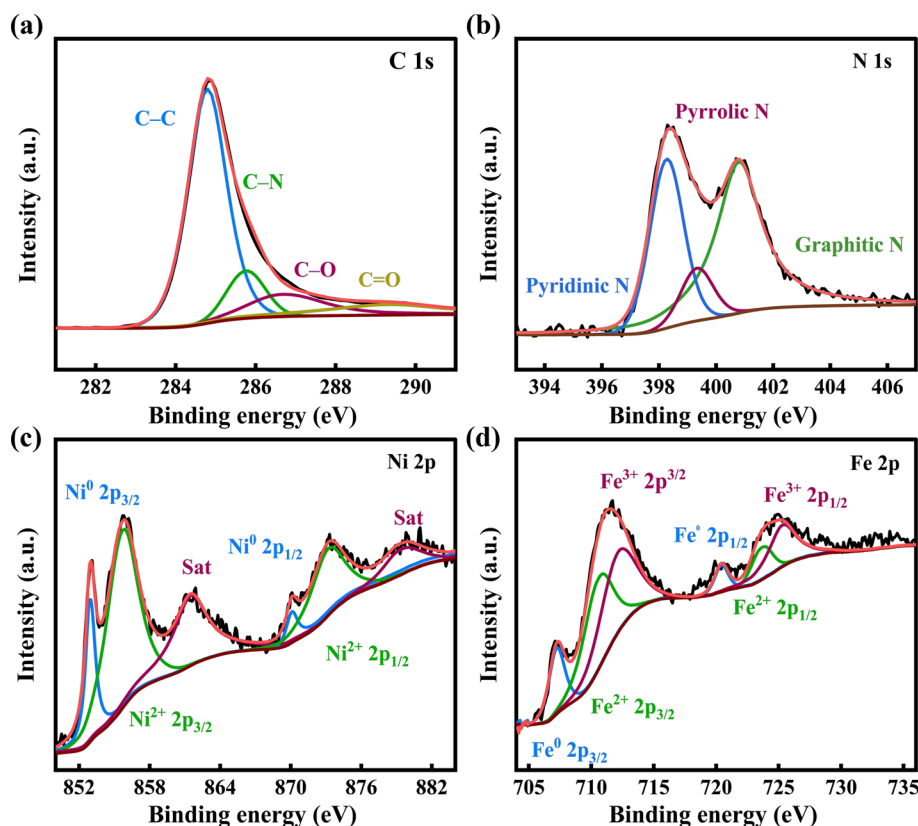
The NO_3RR performance of the NiFe-NFs-X catalysts was investigated using an H-type cell with a three-electrode system in 0.05 mol/L KOH, 0.1 mol/L K_2SO_4, and 0.5 mol/L KNO_3 mixed electrolyte. The linear sweep voltammetry (LSV) curves of NiFe-NF-X were plotted to compare the catalyst activity (Fig. 3a). The results revealed that NiFe-NFs-2 has a lower onset potential than other catalysts. At the same potentials, the NiFe-NFs-2 exhibited a higher current density than other catalysts.

The LSV curves of NiFe-NFs-2 in mixed electrolyte with or without 0.5 mol/L NO_3^- were investigated. The NiFe-NFs-2 exhibited a larger current density and lower onset potential in the electrolyte system containing NO_3^- than without NO_3^-, indicating the occurrence of NO_3RR in the electrolytic system (Fig. S10). Subsequently, the Faradaic efficiency and yield of NH_3 of NiFe-NFs-2 at various potentials were further investigated using chronoamperometry (CA), and the NH_3 generated was quantified using the indophenol blue method (standard curve in Fig. S11). The current density and NH_3 yield gradually increased with the increase of cathode potential (Fig. S12). However, the Faradaic efficiency of NH_3 declined at higher potential due to the severe side reaction of hydrogen evolution. Simultaneously, bubbles can be observed on the working electrode during electrolysis. The results revealed that NiFe-NFs-2 had the best performance with a Faradaic efficiency of 94.3% and

an ammonia production performance of 10,489 μg/(h·mg) at −0.645 V vs. RHE. Meanwhile, NiFe-NFs-2 exhibited the highest Faradaic efficiency and catalytic activity than other catalysts (Figs. 2b, S13). To further validate the N source of NH_3, we tested without NO_3^- and with 0.5 mol/L KNO_3 electrolytes. Only trace amounts of NH_3 were detected without NO_3^- electrolyte, and its current density was considerably smaller than that in the 0.5 mol/L KNO_3 electrolyte (Fig. S14). The above results showed that the rough surface of NiFe-NF-2 favors mass transfer.

Durability is another important characteristic of electrocatalyst, and the endurance cycle test of NiFe-NFs-2 was carried out at − 0.645 V. After six cycles (0.5 h each) (Fig. 3c), indicating that NiFe-NFs-2 had good electrochemical stability. There were no significant fluctuations in ammonia yield and Faradaic efficiency. In the long-term stability test of 12 h, we can see a slight decrease in the current density of the reaction. (Fig. S15). SEM showed that the slight decrease in current was mainly due to the slight shedding of particles. (Fig. S16a). After the NO_3RR stability tests, the XPS confirmed that the valence chemical states were well-preserved (Fig. S17). Considering the favorable NO_3RR activity and good stability, NiFe-NFs-2 can be a promising catalyst for efficient NO_3RR electrocatalysis.

Furthermore, the OER electrocatalytic activity of the prepared catalysts was evaluated using LSV at a scan rate
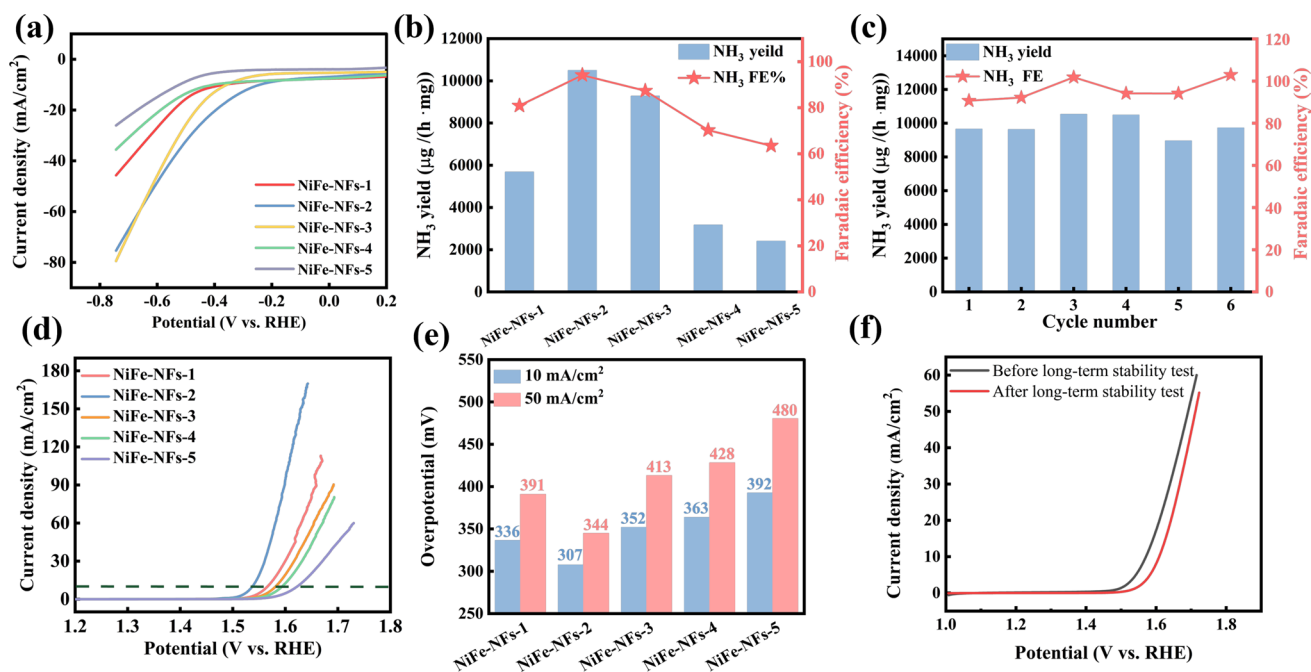
Fig. 3 **a** LSV curves of NiFe-NFs-*X* in 0.05 mol/L KOH, 0.1 mol/L K_2SO_4 and 0.5 mol/L KNO_3 mixed electrolyte. **b** FE and yield rate of NH_3 for the prepared NiFe-NFs-*X* at −0.654 V (vs. RHE). **c** Cycling tests of NiFe-NFs-2 at −0.645 V. **d** OER polarization curves of vari-ous catalysts in 1.0 mol/L KOH with IR compensation. **e** Overpotential of different catalysts at 10 and 50 mA/cm² for OER. **f** LSV plots before and after chronoamperometric tests of OER

of 10 mV/s in 1.0 mol/L KOH electrolyte. The LSV curves (Fig. 3d) showed that NiFe-NFs-2 had the lowest onset potential. Compared to other materials, NiFe-NFs-2 exhibited a low overpotential of 307 mV at 10 mA/cm², which was lower than those of NiFe-NFs-1 (336 mV), NiFe-NFs-3 (352 mV), NiFe-NFs-4 (363 mV), and NiFe-NFs-5 (392 mV). The OER overpotential of the 5 kinds of catalysts was compared at high current density (Fig. 3e). It was found that the OER activity of NiFe-NFs-2 remained outstanding at a high current density of 50 mA/cm². The NiFe-NFs-2 showed strong electrochemical durability as verified by the chronoamperometric response (Fig. S18). The favorable stability of NiFe-NFs-2 can result from its robust structure, as confirmed by the well-preserved morphology and the valence chemical states after the stability tests (Figs. S16b, S19). The LSV curve of the before and after stability test was not much different (Fig. 3f). This result suggested that the NiFe-NFs-2 also has better stability for OER: the specific structure and outstanding mass transfer attributed to the excellent performance.

To further investigate the excellent performance of NiFe-NFs-2, we found that the Tafel slope (Fig. 4a) of NiFe-NFs-2 was 44.2 (mV/dec), which was lower than those of NiFe-NFs-1 (56.2 mV/dec), NiFe-NFs-3 (58.1 mV/dec),

NiFe-NFs-4 (66.7 mV/dec), and NiFe-NFs-5 (78.8 mV/dec), indicating that NiFe-NFs-2 had the fastest OER reaction kinetics. Furthermore, the Tafel slope value was close to 40 mV/dec, indicating the rate determining step was $M + OH^- − e^- = M–OH$. Thus, OH^- mass transfer would improve the OER performance. Furthermore, electrochemical impedance spectroscopy tests were performed, where the intersection of the real axis with the starting point of the Nyquist plots represents the solution resistance (R1), and the semicircle diameter represents the charge transfer resistance (R2). The Nyquist plot showed that the internal resistance of NiFe-NFs-2 is as low as 12.1 Ω, considerably lower than those of NiFe-NFs-1 (29.8 Ω), NiFe-NFs-3 (33.4 Ω), NiFe-NFs-4 (50.2 Ω), and NiFe-NFs-5 (75.9 Ω) (Figs. 4b, S20). Consequently, NiFe-NFs-2 had a lower charge transfer resistance and a faster charge transfer rate. Theoretically, the electrochemically active surface area (ECSA) is linearly related to the C_{dl} value, so the ECSA of different materials can be obtained by comparing their C_{dl} values. The C_{dl} value of NiFe-NFs-2 (5.34 mF/cm²) was significantly greater than those of the other prepared catalysts (Figs. 4c, S21). The Brunauer–Emmett–Teller measurements showed that NiFe-NFs-2 has a surface area of 461.547 m²/g, which is higher than those of NiFe-NFs-1 (444.557 m²/g), NiFe-NFs-3
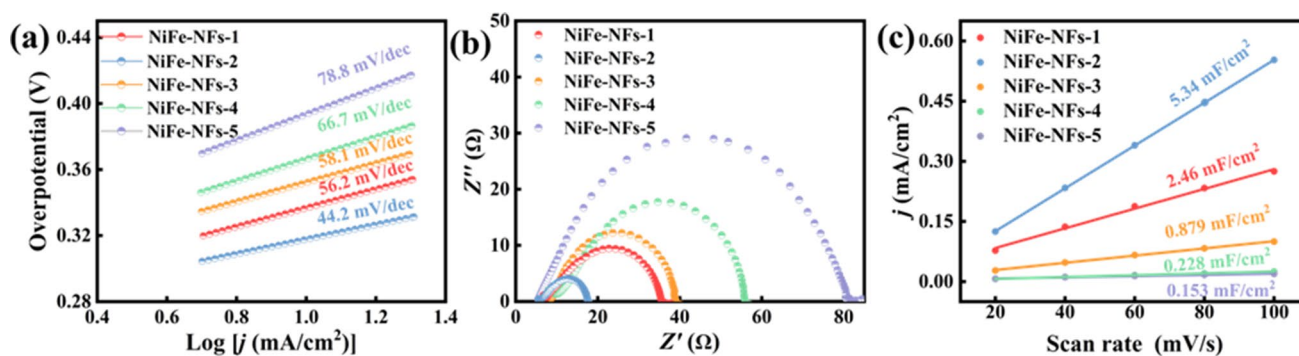
Fig. 4 **a** Tafel plots of different catalysts. **b** Nyquist plots of prepared samples at 1.55 V (vs. RHE). **c** Capacitive currents at different scan rates of different catalysts

(427.793 m^2/g), NiFe-NFs-4 (360.151 m^2/g) and NiFe-NFs-5 (313.824 m^2/g) (Fig. S22). The large specific surface area of the catalyst facilitates the escape of the gases generated by the catalytic reaction and increases the exchange rate of the electrolyte over the catalyst [39]. The suitable preoxidation heating rate provides a larger electroactive surface for the OER, resulting in excellent OER performance of NiFe-NFs-2. With the same load, the modulation of NF diameter exposes NiFe-NF-2 to more electrocatalytic active sites and a larger interfacial contact area with the electrolyte, thus showing a higher activity. Combined with experimental results and characterization results, we can conclude that due to the rough surface structure of NiFe-NPs-2, the catalyst has a large specific surface area, promoting the mass transfer process and producing a high catalytic activity.

Conclusions

We successfully prepared NiFe nanoparticle-doped NFs by electrospinning technology and a two-step pyrolysis method. Morphological and structural characterization indicated that the NiFe-NFs-2 surface is rougher than the compared catalyst. The NiFe-NFs-2 excellent structure and properties of NiFe-NFs-2 contribute to a high FE (94.3%), ammonia yield (10,489 μg/(h·mg)) for NO_3RR, and low onset potential (307 mV) for OER. Furthermore, Tafel and ECSA experiments confirmed that a rougher surface can benefit a highly exposed active site and rapid mass transfer process. This research has offered novel ideas by improving the mass transfer process to enhance the catalytic capacity in NO_3RR and OER.

Declarations

Conflict of interest The authors declare that there is no conflict of interest.

References

1. Xu H, Ma YY, Chen J et al (2022) Electrocatalytic reduction of nitrate: a step towards a sustainable nitrogen cycle. Chem Soc Rev 51(7):2710–2758
2. Liu JX, Richards D, Singh N et al (2019) Activity and selectivity trends in electrocatalytic nitrate reduction on transition metals. ACS Catal 9(8):7052–7064

3. Zheng WX, Zhu LY, Yan Z et al (2021) Self-activated Ni cathode for electrocatalytic nitrate reduction to ammonia: from fundamentals to scale-up for treatment of industrial wastewater. Environ Sci Technol 55(19):13231–13243

4. Wang YY, Zhang LL, Niu YJ et al (2021) Boosting NH_3 production from nitrate electroreduction via electronic structure engineering of Fe_3C nanoflakes. Green Chem 23(19):7594–7608

5. Xue YH, Yu QH, Ma QA et al (2022) Electrocatalytic hydrogenation boosts reduction of nitrate to ammonia over single-atom Cu with Cu(I)–N_3C_1 sites. Environ Sci Technol 56(20):14797–14807

6. Wang J, Wu DJ, Li MH et al (2022) Bismuth ferrite as an electrocatalyst for the electrochemical nitrate reduction. Nano Lett 22(13):5600–5606

7. Zhao J, Zhang JJ, Li ZY et al (2020) Recent progress on NiFe-based electrocatalysts for the oxygen evolution reaction. Small 16(51):2003916

8. Zeng F, Mebrahtu C, Liao LF et al (2022) Stability and deactivation of OER electrocatalysts: a review. J Energy Chem 69:301–329

9. Li HX, Han XE, Zhao W et al (2022) Electrochemical preparation of nano/micron structure transition metal-based catalysts for the oxygen evolution reaction. Mater Horiz 9(7):1788–1824

10. Shinde PV, Samal R, Rout CS (2022) Comparative electrocatalytic oxygen evolution reaction studies of spinel $NiFe_2O_4$ and its nanocarbon hybrids. Trans Tianjin Univ 28(1):80–88

11. Zhu JY, Xue Q, Xue YY et al (2020) Iridium nanotubes as bifunctional electrocatalysts for oxygen evolution and nitrate reduction reactions. ACS Appl Mater Interfaces 12(12):14064–14070

12. Li L, Cao XJ, Huo JJ et al (2023) High valence metals engineering strategies of Fe/Co/Ni-based catalysts for boosted OER electrocatalysis. J Energy Chem 76:195–213

13. Han JY, Guan JQ (2023) Multicomponent transition metal oxides and (oxy)hydroxides for oxygen evolution. Nano Res 16(2):1913–1966

14. Wang CQ, Zhang YB, Luo HX et al (2022) Iron-based nanocatalysts for electrochemical nitrate reduction. Small Methods 6(10):2200790

15. Yang XL, Ben HX, Ragauskas AJ (2021) Recent advances in the synthesis of deuterium-labeled compounds. Asian J Org Chem 10(10):2473–2485

16. Li XH, Ran FT, Yang F et al (2021) Advances in mxene films: synthesis, assembly, and applications. Trans Tianjin Univ 27(3):217–24717

17. Niu ZD, Fan SY, Li XY et al (2022) Bifunctional copper-cobalt spinel electrocatalysts for efficient tandem-like nitrate reduction to ammonia. Chem Eng J 450:138343

18. Oh NK, Seo J, Lee SJ et al (2021) Highly efficient and robust noble-metal free bifunctional water electrolysis catalyst achieved via complementary charge transfer. Nat Commun 12(1):1–12

19. Song QN, Zhang S, Hou XS et al (2022) Efficient electrocatalytic nitrate reduction via boosting oxygen vacancies of TiO_2 nanotube array by highly dispersed trace Cu doping. J Hazard Mater 438:129455

20. Li Y, Wang TZ, Asim M, Pan L et al (2022) Manipulating spin polarization of defected Co_3O_4 for highly efficient electrocatalysis. Trans Tianjin Univ 28(3):163–17321

21. Zhao YL, Liu Y, Zhang ZJ et al (2022) Flower-like open-structured polycrystalline copper with synergistic multi-crystal plane for efficient electrocatalytic reduction of nitrate to ammonia. Nano Energy 97:107124

22. Liang Y, Han YF, Li JS et al (2022) Wettability control in electrocatalyst: a mini review. J Energy Chem 70:643–655

23. He WH, Zhang J, Dieckhöfer S et al (2022) Splicing the active phases of copper/cobalt-based catalysts achieves high-rate tandem electroreduction of nitrate to ammonia. Nat Commun 13(1):1129

24. Liu ZB, Yu C, Han XT et al (2016) CoMn layered double hydroxides/carbon nanotubes architectures as high-performance electrocatalysts for the oxygen evolution reaction. ChemElectroChem 3(6):906–912

25. Wei P, Sun XP, Liang QR et al (2020) Enhanced oxygen evolution reaction activity by encapsulating NiFe alloy nanoparticles in nitrogen-doped carbon nanofibers. ACS Appl Mater Interfaces 12(28):31503–31513

26. Zhu H, Yu DN, Zhang SG et al (2017) Electrocatalysis: morphology and structure engineering in nanofiber reactor: tubular hierarchical integrated networks composed of dual phase octahedral $CoMn_2O_4$/carbon nanofibers for water oxidation. Small 13(26):1700468

27. Lan YE, Luo HX, Ma YY et al (2021) Synergy between copper and iron sites inside carbon nanofibers for superior electrocatalytic denitrification. Nanoscale 13(22):10108–10115

28. Mao H, Fu YL, Yang HR et al (2020) Ultrathin 1T-MoS_2 nanoplates induced by quaternary ammonium-type ionic liquids on polypyrrole/graphene oxide nanosheets and its irreversible crystal phase transition during electrocatalytic nitrogen reduction. ACS Appl Mater Interfaces 12(22):25189–25199

29. Wang Z, Sun CC, Bai XX et al (2022) Facile synthesis of carbon nanobelts decorated with Cu and Pd for nitrate electroreduction to ammonia. ACS Appl Mater Interfaces 14(27):30969–30978

30. Fang Y, Xue YR, Li YJ et al (2020) Graphdiyne interface engineering: highly active and selective ammonia synthesis. Angew Chem Int Ed 59(31):13021–13027

31. Jia Y, Xiong XY, Wang DN et al (2020) Atomically dispersed Fe–N_4 modified with precisely located S for highly efficient oxygen reduction. Nano Micro Lett 12(1):1–13

32. Tian YH, Xu L, Li M et al (2020) Interface engineering of CoS/CoO@N-doped graphene nanocomposite for high-performance rechargeable Zn–air batteries. Nano Micro Lett 13(1):1–15

33. Li XG, Zhou JH, Liu C et al (2021) Encapsulation of Janus-structured Ni/Ni_2P nanoparticles within hierarchical wrinkled N-doped carbon nanofibers: interface engineering induces high-efficiency water oxidation. Appl Catal B 298:120578

34. Lai CL, Fang JY, Liu XP et al (2021) in situ coupling of NiFe nanoparticles with N-doped carbon nanofibers for Zn-air batteries driven water splitting. Appl Catal B 285:119856

35. Li MX, Zhu Y, Wang HY et al (2019) Ni strongly coupled with Mo_2C encapsulated in nitrogen-doped carbon nanofibers as robust bifunctional catalyst for overall water splitting. Adv Energy Mater 9(10):1803385

36. Lan YE, Chen JL, Zhang H et al (2020) Fe/Fe_3C nanoparticle-decorated N-doped carbon nanofibers for improving the nitrogen selectivity of electrocatalytic nitrate reduction. J Mater Chem A 8(31):15853–15863

37. Wang CH, Yang HC, Zhang YJ et al (2019) NiFe alloy nanoparticles with hcp crystal structure stimulate superior oxygen evolution reaction electrocatalytic activity. Angew Chem Int Ed 58(18):6099–6103

38. Li ZY, Liang X, Gao QM et al (2019) Fe, N co-doped carbonaceous hollow spheres with self-grown carbon nanotubes as a high performance binary electrocatalyst. Carbon 154:466–477

39. Lv XW, Liu YP, Hao R et al (2020) Urchin-like Al-doped Co$_3$O$_4$ nanospheres rich in surface oxygen vacancies enable efficient ammonia electrosynthesis. ACS Appl Mater Interfaces 12(15):17502–17508
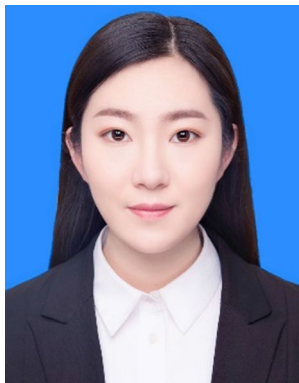
Haibo Huang received her Ph.D. degree from Jilin University in 2016 and joined Dalian Institute of Chemical Physics, Chinese Academy of Sciences in 2017 as a postdoctoral fellow. She then became a full Professor and Group Leader of Bio-based Energy Matierials & Devices at NEFU. Her research interests focus on bioinspired construction and application of biomaterials for microscale electrochemical energy storage devices, supercapacitors and batteries.
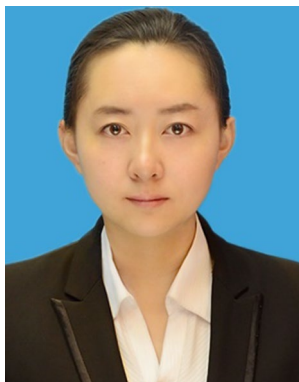
Siqi Li is a lecturer at college of chemistry, chemical engineering and resource utilization, NEFU. She received her Ph.D. (2019) from Jilin University. Her research interests include nanomaterial design and preparation and gas sensor development.

Song Liu is a professor at college of chemistry, chemical engineering and resource utilization, NEFU. He received his B.S. (2014) from Jilin University, and Ph.D. (2020) from Dalian Institute of Chemical Physics, Chinese Academy of Sciences (DICP, CAS). His research interests include high value utilization of biomass, CO$_2$/N$_2$/H$_2$O electrochemical conversion reaction.

Authors and Affiliations

Yan Li[1] · Ziwang Kan[1] · Lina Jia[1] · Dan Zhang[1] · Yan Hong[1] · Jingjing Liu[1] · Haibo Huang[2] · Siqi Li[1] · Song Liu[1]

✉ Haibo Huang
   supernova_bo@163.com

✉ Siqi Li
   lisiqi@nefu.edu.cn

✉ Song Liu
   carlosliusong@nefu.edu.cn

[1] College of Chemistry, Chemical Engineering and Resource Utilization, Northeast Forestry University, Harbin 150040, China

[2] Department of Materials Science and Engineering, Northeast Forestry University, Harbin 150040, China